(Preprint) AAS 19-714

OSIRIS-REX ORBIT DETERMINATION PERFORMANCE DURING THE NAVIGATION CAMPAIGN

Jason M. Leonard[*], Jeroen L. Geeraert[†], Brian R. Page[†], Andrew S. French[‡], Peter G. Antreasian[‡], Coralie D. Adam[§], Daniel R. Wibben[¶], Michael C. Moreau[‖], and Dante S. Lauretta[**]

The OSIRIS-REx mission Navigation Campaign consists of three sub-phases: Approach, Preliminary Survey, and Orbital A. Approach was designed for initial characterization of Bennu while matching Bennu's heliocentric velocity. Preliminary Survey provided the first spacecraft-based estimate of Bennu's mass. This phase consisted of five target flybys with a close approach distance of about 7 km. Orbital A was a two-month phase devoted to the Navigation Team learning the close proximity operations dynamics and environment around Bennu and transitioning from center-finding optical navigation to landmark feature-based navigation. This paper provides a detailed summary of the orbit determination performance throughout the Navigation Campaign.

INTRODUCTION

The Origins, Spectral Interpretation, Resource Identification, and Security–Regolith Explorer (OSIRIS-REx) mission is the first American asteroid-sample-return endeavor;[1] its target is (101955) Bennu.[2] The OSIRIS-REx spacecraft launched in September 2016 and was in cruise operations until August 2018.[3,4] The first image of Bennu was recorded on OSIRIS-REx's PolyCam high-resolution imager on August 17, 2018 initiating the start of the Navigation Campaign.[5,6] The Navigation Campaign consists of three sub-phases that initiated proximity operations (ProxOps) at Bennu: Approach, Preliminary Survey, and Orbital A.

Approach was designed for initial characterization of Bennu while speeding up from interplanetary cruise to match the orbital velocity of Bennu. Initial optical images of Bennu as a point source gave the Orbit Determination (OD) team the necessary measurements to begin estimating the orbital ephemeris of Bennu.[7] Maneuvers throughout this phase altered the approach trajectory to provide the parallax necessary to reduce the radial uncertainty to Bennu in order to target final Approach phase maneuvers for the initial characterization flybys. Through high-resolution rotation videos taken during this phase, the OD team estimated the initial spin-state to determine if Bennu was in principal axis rotation or non-principal axis rotation (wobble).[8]

Preliminary Survey provided the first spacecraft-based estimate of the mass of Bennu. This phase consisted of five target flybys with a close approach radius of about 7.25 km. Each flyby was designed to obtain detailed imaging of the surface of Bennu from different observing conditions. The first three flybys were over Bennu's

[*] Orbit Determination Team Lead, OSIRIS-REx, KinetX, Inc., Space Navigation and Flight Dynamics Practice, 21 W. Easy St., Ste 108, Simi Valley, CA 93065, USA.
[†] Orbit Determination Analyst, OSIRIS-REx, KinetX, Inc., Space Navigation and Flight Dynamics Practice, 21 W. Easy St., Ste 108, Simi Valley, CA 93065, USA.
[‡] Navigation Team Chief, OSIRIS-REx, KinetX, Inc., Space Navigation and Flight Dynamics Practice, 21 W. Easy St., Ste 108, Simi Valley, CA 93065, USA.
[§] Optical Navigation Team Lead, OSIRIS-REx, KinetX, Inc., Space Navigation and Flight Dynamics Practice, 21 W. Easy St., Ste 108, Simi Valley, CA 93065, USA.
[¶] Trajectory and Maneuver Team Lead, OSIRIS-REx, KinetX, Inc., Space Navigation and Flight Dynamics Practice, 21 W. Easy St., Ste 108, Simi Valley, CA 93065, USA.
[‖] Flight Dynamics System Lead, NASA/GSFC Navigation and Mission Design Branch, 8800 Greenbelt Rd, Greenbelt, MD 20771, USA.
[**] Principal Investigator, Lunar and Planetary Laboratory, University of Arizona, 1415 N 6th Ave, Tucson, AZ 85705, USA.

north pole, followed by a transit to the equator for the fourth flyby, then a transit to the south pole for the final flyby. Each flyby provided additional information on the mass of Bennu. Successful completion of this phase meant the OD team's confidence in the mass estimate would be less than 1% in error.[9] During the first half of the first flyby, the OD team successfully estimated a mass that was less than 0.25% in error from the refined value achieved later in the Navigation Campaign, and consistent with ground-based mass determination based on the observed Yarkovsky force.[10]

Orbital A was a two-month phase devoted to having the Navigation Team become proficient in navigating in the dynamical environment around Bennu and to successfully transitioning from center-finding optical navigation (OpNav) to landmark-based navigation.[11] The OD team began refining the force models for solar radiation pressure (SRP), spacecraft thermal re-radiation (TRP), and antenna thrust during this phase.[12] In addition to force modeling, the OD team worked closely with the Altimetry Working Group (ALTWG), who were responsible for creating the shape model used for landmark navigation.[13] Estimates of the rotation state of Bennu, deviations in the origin of the shape model figure relative to the center-of-mass, and landmark location errors were fed back to the ALTWG team through several iterations. A center-of-figure to center-of-mass offset of the Bennu reference frame and spin axis was estimated as well as a significant deviation of the spin axis from the estimated spin-state from that predicted based on a constant density shape model.

This paper will provide a detailed summary of the OD performance throughout the Navigation Campaign. An overview is provided of the updates to the spacecraft modeling including SRP, TRP, antenna thrust, the antenna path delays, and Bennu thermal re-radiation (TRR) and their impacts on the navigation. A short treatise on Bennu's pole/wobble, gravity and reference frames is presented. Results from each Navigation Campaign phase are presented. Approach results will focus on initial Bennu spin-state detection and estimation. Reference 5 provided an overview of the initial OD results as well as the OpNav and maneuver performance during the Approach phase. The Preliminary Survey section will focus on initial Bennu mass estimation and flyby prediction performance. Finally, we discuss the Orbital A insertion reconstruction, OpNav performance (center-finding vs landmark), Bennu center-of-figure to center-of-mass offset detection, Bennu gravity and refinement of mass, pole spin-state estimation, SRP refinement, and trajectory prediction performance.

OPTICAL NAVIGATION

OpNav involves the processing and analysis of optical data to assist in determining the trajectory of the spacecraft. While radiometric data are useful in determining the spacecraft position relative to Earth, their use in establishing the spacecraft state relative to other bodies is highly dependent on the *a priori* knowledge of the bodies' physical parameters. For OSIRIS-REx, the uncertainties in Bennu's ephemeris, size, shape, spin-state, and composition were too large to accurately navigate on radiometric data alone; thus, the body-relative OpNav measurements have been essential to performing precision navigation near the asteroid. During outbound cruise, cameras used throughout the Navigation Campaign were calibrated with stellar images to reduce errors in distortion and orientation in the image plane.[14,15] Throughout the Navigation Campaign OpNav images were taken in pairs of one long exposure and one short exposure image. The first step in the OpNav process was to use the background stars in the long exposure images to obtain precise camera attitude solutions. These attitude solutions were obtained by minimizing the differences between star locations and the cataloged star positions utilizing the KinetX Star-Based Image Processing Suite (KXIMP).[7,16,17] The attitude from the long exposure was then propagated to the short exposure epoch to provide highly reliable attitude solutions in the well-exposed asteroid images. Two different OpNav techniques were utilized to generate the measurements used in the OD filter: centroid-based OpNav and landmark-based OpNav.

Centroid-based OpNav

The objective of centroid-based OpNav is to accurately determine the position of the target body center relative to inertial star positions. For the Approach, Preliminary Survey, and Orbital A phases of the OSIRIS-REx mission, KXIMP's center-finding capabilities were utilized to determine the observed (sample, line) location of the Bennu center-of-volume at each image epoch. The center-of-volume derived from the shape model was assumed to be coincident with the center-of-mass until the latter was estimated during Orbital A. The observed (sample, line) location of the Bennu center-of-mass is derived using an appropriate algorithm

depending on whether Bennu is treated as point source or an extended body. During the early Approach phase, when Bennu was less than 3-5 pixels in diameter, it was treated as a point source. In this case, KXIMP determines the centroid using either a least squares fit with a 2D Gaussian point spread function (PSF) or cross-correlation of the camera PSF with the point-source signal. From mid-Approach onward, once Bennu extended beyond 5 pixels in the image, it was treated as an extended body and the centroid was found from a cross-correlation with a simulated image of the best available shape model and spin-state parameters.

Landmark-based OpNav

Once global imaging data and digital terrain maps (DTMs) were available in the Orbital A mission phase, the Navigation Team began the transition from using centroid-based OpNav to using landmark-based OpNav. In landmark-based OpNav the observed (sample, line) locations of many landmarks are determined by cross-correlating image data with DTMs rendered with predicted lighting geometries. Landmarks do not necessarily refer to an obviously identifiable feature, such as a crater or boulder, but instead refer to the center of a small section of the surface. The surface sections are referred to as a maplets, which consist of a combination of DTMs and relative albedo maps with the "landmark" being the center of the maplet. Landmark-based OpNav utilizes the stereophotoclinometry (SPC; see Reference 18) software suite applicable to navigation.[7]

Landmark-based OpNav yields the higher navigation accuracy required for close proximity science observations. This transition was the primary objective of the Orbital A phase; moving on to the Site Selection Campaign was contingent on a successful completion of the transition. During the four-week transition period, both centroid-based and landmark-based OpNav solutions were processed and delivered to the OD team. The centroid-based solutions were used as the baseline solutions in OD until the landmark-based solutions had a long enough data arc and their performance was verified. On 25 January 25 2019 the Navigation Team made the official transition to baseline the landmark-based OpNav solutions.

SPACECRAFT MODELING

Due to the small size and mass of Bennu, the knowledge of non-gravitational forces such as SRP, spacecraft TRP, antenna pressure and path delays, as well Bennu TRR, becomes exceedingly important for predicting the spacecraft state and estimating Bennu's geophysical parameters. Figure 1 illustrates the magnitude of the forces experienced by OSIRIS-REx spacecraft during the Orbital A Phase, where SRP is the largest next to the gravitational parameter (GM) of Bennu, followed by TRP on the order of 10% of the SRP acceleration. A high-level overview of these force models is outlined. A more detailed description of the modeling of SRP, TRP, and antenna pressure with results concerning predicted trajectory performance is given in Reference 12.

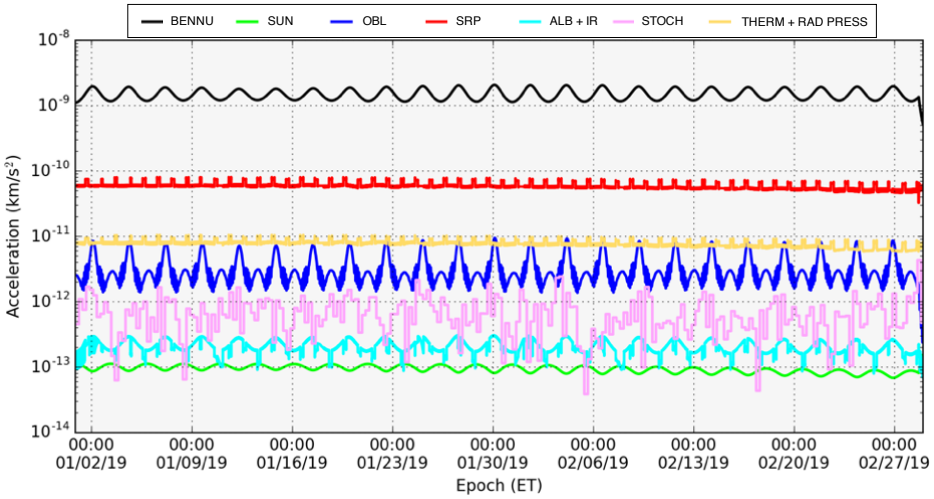

Figure 1: Orbital A phase force magnitudes on OSIRIS-REx (BENNU = Central body-Bennu, SUN = Sun third body, OBL = Bennu oblateness, SRP = solar radiation pressure, ALB + IR = Bennu thermal re-radiaion, STOCH = stochastic accelerations, THERM + RAD PRESS = spacecraft thermal re-radiation + antenna/LIDAR pressure)

Solar Radiation Pressure

Throughout the Navigation Campaign of the OSIRIS-REx mission, gradual yet significant improvements were made to the SRP models. For the duration of cruise and Approach, a 10-plate representation was used to model the SRP accelerations imparted on the spacecraft. This 10-plate model used fitted optical (specular and diffuse) values from early on in cruise and approximated areas for each of the panels based on the best knowledge of the spacecraft dimensions available to the Navigation Team at that time.

During the Orbital A phase, at attitudes other than Sun-point (HGA directed at the Sun), some mismodeling became apparent as residual large stochastics accelerations were estimated. This was especially prominent during the HGA passes, with the spacecraft at Earth-point. Two avenues were pursued to improve the SRP models with different levels of effort and timelines. One was to continue using the plate model but include an accurate model of the HGA radome, while the other was to use a ray-traced SRP model. The ray-traced SRP model was an iterative approach and included various models of the spacecraft with different fidelity levels. Ultimately, a very high-fidelity model was used to perform the SRP ray-tracing analysis. The ray-traced model ingested the same optical properties as those used from the 10-plate model, and considered multiple ray bounces between the various surfaces. Due to the unknown error associated with the optical properties associated with the ray-traced model, an SRP scale factor was still estimated as well. The ray-traced model is the highest fidelity SRP model available to the OD team and was approximated using a 10x10 spherical harmonics representation or a 4π steradian interpolated tabular model. The error in the approximation of these two representations compared to the actual ray-traced model was negligible for the attitudes experienced by the spacecraft. When comparing the predicted spacecraft state performance averaged over a 5-day window, there was nearly a 3-fold improvement from the standard 10-plate model to the tabular SRP representation based on the ray-traced model.[12]

Thermal Radiation Pressure

As indicated by Figure 1, the TRP acceleration imparted on the spacecraft is approximately 10% of the SRP acceleration. The spacecraft TRP model is based on the temperature profile of the spacecraft surfaces at various illuminating conditions over assorted Sun-spacecraft distances. The temperature profile is determined using a high-fidelity thermal model of the spacecraft that is informed by onboard temperature sensors. This temperature profile is then fit using splines such that it can be interpolated for any illuminating condition and Sun-spacecraft distance. During cruise and early on in the Approach phase the TRP model consisted of 10 plates, similar to the original SRP 10-plate model. However, to improve the accuracy of the TRP model, the large radiators located on the $-$Z deck were modeled as separate plates instead of being combined with the average temperature of the $-$Z deck. Furthermore, because the shape of the HGA radome had a large effect on the SRP model, it was assumed that neglecting to properly model the HGA in the thermal model could also be a significant source of error. Consequently, the HGA shape was added and modeled as hundreds of individual plates and checked for the self-shadowing condition. From there, knowing all of the plates' areas, emissivities, and temperatures, the thermal acceleration is computed.

Antenna Pressure

Power is continually radiating from either the high-gain antenna (HGA) or low-gain antennas (LGAs) at a steady 100 W. Perturbative effects of antenna radiation on the orbit of an artificial satellite are well known and applied in the GPS literature.[19,20] The maximum acceleration of a radiating antenna, a_{rad}, is given by

$$a_{rad} = \frac{P_{ant}}{m \cdot c} \tag{1}$$

where P_{ant} is the power of the antenna, m is the spacecraft mass, and c is the speed of light. Due to the large half-power beam width of the LGA, Eq. 1 would need to take into account the drop off in acceleration due the radiation not being directed at a single point. Reference 21 attempted to expand on Eq. 1 and derive the antenna radiation pressure equations necessary to account for the antenna beam pattern. Unfortunately the article contained a number of inaccuracies, so the OD team re-derived the antenna pressure with a known antenna gain pattern independently.[12] Using the correct equation for antenna pressure, the HGA was computed

to impart an acceleration of 2.4×10^{-13} km/s^2. The LGA acceleration is lower at 2.2×10^{-13} km/s^2 due to the wider half-power beam width. In addition to the antennas, the LIDAR instrument also radiates at a power of 100 W and is also taken into account when it is on.

Antenna Path Delay

During cruise occasional biases became apparent when switching from one antenna to another. It was determined that the cause of these biases were electronic path delays due to slightly alternate routes of the antennas that were not accurately measured in ground testing of the telecom system. The OD team estimated biases for the +X LGA, −X LGA, and medium-gain antenna (MGA) relative to the measured HGA path delay. The +X LGA antenna path delay error was estimated at -4.1 ± 0.4 RU. The other antennas, the −X LGA and the MGA were also estimated at -6.08 ± 5.0 RU and -6.9 ± 2.2 RU respectively relative to the values provided pre-launch from the telecom team.

Bennu Thermal Re-Radiation

For the Navigation Campaign, the OD team implemented a variation of the Standard Thermal Model (STM; see Reference 22) and Near-Earth Asteroid Thermal Model (NEATM; see Reference 23) for determining the acceleration on the spacecraft due to thermal emissions of reflected and infrared radiation of the surface. The acceleration due to TRR while in a terminator orbit during the Orbital A phase varied between 1.0×10^{-13} km/s^2 to 3.0×10^{-13} km/s^2, the same order of magnitude as the antenna pressure. The implemented thermal model computes the surface temperature as

$$T(i) = T_{SS} \cos^{1/4}(i), \quad 0 \leq i \leq \pi/2, \tag{2}$$

where i is the angle between a point on the surface and the subsolar point. T_{SS} is the temperature of the subsolar point and is expressed as

$$T_{SS} = \left(\frac{(1 - a_b) G_R}{\epsilon \sigma_B} \right) \tag{3}$$

where a_b is the bold albedo, G_R is the solar flux at a distance R from the Sun, ϵ is the emissivity of the surface, and σ_B is the Boltzmann constant. The STM and NEATM assume a peak temperature occurring at the subsolar point and do not take into account the thermal inertia of the surface.[24] The thermal inertia is a measure of the retention of heat of the surface as the asteroid rotates through a full revolution. When a body has a significant thermal inertia, the peak temperature moves in longitude but at a certain angle.[25] This more advanced representation will be used in subsequent orbital phases where the spacecraft is closer to the surface and has larger excursions from the terminator plane. However, for the Navigation Campaign, the STM and NEATM are accurate enough for short- and long-term trajectory predictions.

BENNU GEOPHYSICAL MODELING

The accurate modeling of Bennu's geophysical parameters is a necessary undertaking in order for the OSIRIS-REx mission to have a successful Touch and Go (TAG) sample acquisition event. The Navigation Team is required to supply a gravity field, evaluation of the shape, estimates of the spin-state, and any anomalies determined between the constant density shape model assumption and what is evaluated with inflight data. Bennu, even though it had never been encountered by a spacecraft prior to the arrival of OSIRIS-REx, has been categorized extensively by remote observations from Earth.[2,26]

Pre-encounter measurements indicated that Bennu is a B-type asteroid (see Reference 27 and 28) with an average radius of ∼250 m and an equatorial radius of ∼275 m based on ground-based radar observations and shape inversion.[26] The rotation period of Bennu prior to encounter was well-known with a rotation rate of 1 revolution every 4.3 hours.[29] The same radar and lightcurve analysis estimated an inertial spin rate of 2010.489 ± 0.94 deg/day and spin axis with right ascension of 86.6388 deg and a declination of -65.1086 deg relative to the International Celestial Reference Frame (ICRF) with an uncertainty of 4 degrees.[2,26,29] This 4 degree uncertainty cannot exclude the potential that Bennu is in non-principal axis rotation as other small bodies have shown properties of non-principal axis rotation.[30–32] Using detailed rotation measurements

in 1999, 2005, and 2012 indicating that Bennu's rotation rate has increased over the past two decades, Reference 33 estimated the a spin rate acceleration of $2.64 \pm 1.05 \times 10^{-6}$ deg/day^2. Reference 34 updated the estimated acceleration to $3.63 \pm 0.52 \times 10^{-6}$ deg/day^2 utilizing Approach phase lightcurve data. The ephemeris of Bennu was known to a few kilometers prior to Approach based on observations spanning several years.[10] A byproduct of the ephemeris estimation produced a novel approach to estimate the mass of Bennu based on the drift of the trajectory over many years. This drift, attributed to the Yarkovsky effect (see Ref. 35), allowed for a direct measurement of the GM of Bennu to be 5.2 ± 0.6 m^3/s^2.[10]

Pole and Wobble Modelling

Bennu's inertial orientation is defined by the location of the pole and equator relative to the ICRF. Typically, the IAU uses two angles to define the orientation of the pole: the right ascension of the pole, α; and the declination of the pole, δ. The prime meridian location is defined by W and its angular separation from the IAU defined vector Q (where the ICRF equator intersects Bennu's equator). Figure 2 shows the IAU defined definitions and orientations necessary to express the rotation state of an asteroid relative to the ICRF.[36] The initial values for the right ascension and declination are typically given at the epoch of J2000 (1 January 2000, 12:00:00 TDB). Principal axis rotation occurs when the body is spinning around a single principal axis of inertia where the most stable condition occurs when the rotation axis is about the maximum moment of inertia. If the body is in principal axis rotation, no rate terms will be given for α and δ.

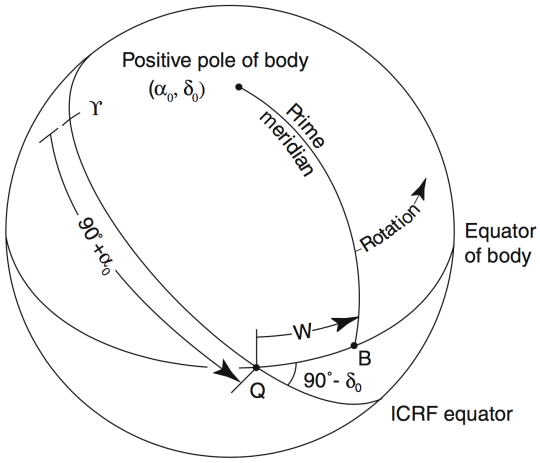

Figure 2: IAU definition of the inertial orientation of an asteroid in the ICRF utilizing the three defining angles: α, δ and W.[36]

Typically, external torques acting on a body induce small rotations about other principal axes. An asteroid can become rotationally excited due to external torque mechanisms such as Yarkovsky–O'Keefe–Radzievskii–Paddack (YORP, see Reference 32) or changes in its principal moments of inertia. Pre-encounter ground-based radar imaging did not show any presence of non-principal axis rotation; however, there remained a large uncertainty in the estimate of the rotation axis.[26] Wobble of the pole can be characterized by a rotation about all three body-fixed axes with the location of the instantaneous spin axis changing in the Bennu-fixed frame. In order to model any potential spin-state accurately, the Euler equations of rigid body motion are integrated according to

$$\dot{\boldsymbol{\omega}}(t) = \mathbf{I}^{-1}\left[\mathbf{R}^T(t)\tilde{\boldsymbol{\tau}}(t) - \boldsymbol{\omega}(t) \times \mathbf{I}\boldsymbol{\omega}(t)\right] \tag{4}$$

where $\dot{\boldsymbol{\omega}}(t)$ is the angular acceleration, $\mathbf{I}$ is the body's inertia tensor, $\tilde{\boldsymbol{\tau}}(t)$ is any external torque acting on the body in the body-fixed frame, $\mathbf{R}(t)$ is the rotation matrix from the inertial frame to the body-fixed spin-axis frame, and $\boldsymbol{\omega}(t)$ is the angular velocity vector. This equation is integrated along with a set of quaternions defining the rotation matrix from the inertial frame to the body-fixed spin-axis frame to completely define the orientation angles $\alpha(t)$, $\delta(t)$ and $W(t)$. Reference 8 analyzed the potential for wobble in the case of Bennu

and how accurately a simple principal axis rotation model could recover the rotation state. With a 1 degree wobble, Reference 8 showed that the best a principal axis rotation model could recover would result in $\sim$1 m error on the surface of Bennu. Shape model resolutions for the Navigation Campaign range from 0.35 cm to 1.5 m per pixel. In order to estimate the position of the spacecraft accurately and to be able to estimate the dynamics and geophysical environment of Bennu from landmark based images, a detailed representation of the spin-state of Bennu is necessary. In order to achieve this level of accuracy and to mitigate any other potential frame and orientation issues that could arise during the shape-model building, the OD team defines an additional rotation matrix from the body-fixed spin-axis frame to the shape-model-defined body-fixed frame to account for any discrepancy in the location of the spin axis as defined by the +Z axis of the shape-model-defined reference frame.

Gravity

The *a priori* gravity field used for ProxOps was derived from the *a priori* shape model from Reference 26 and assumed that the asteroid was constant density.[37] A 16x16 spherical harmonic gravity field was generated with the prime meridian defined by the *a priori* shape model frame. This gravity model was only used for covariance and Monte-Carlo analysis done prior to ProxOps. Once initial shape models were generated by the ALTWG team, the 16x16 constant density gravity model was updated. Figure 3 shows the radial gravity acceleration mapped to a 290 m sphere with the point-mass gravity removed. The variations in the gravity field at this distance are only on the order of 1.3 mGal.

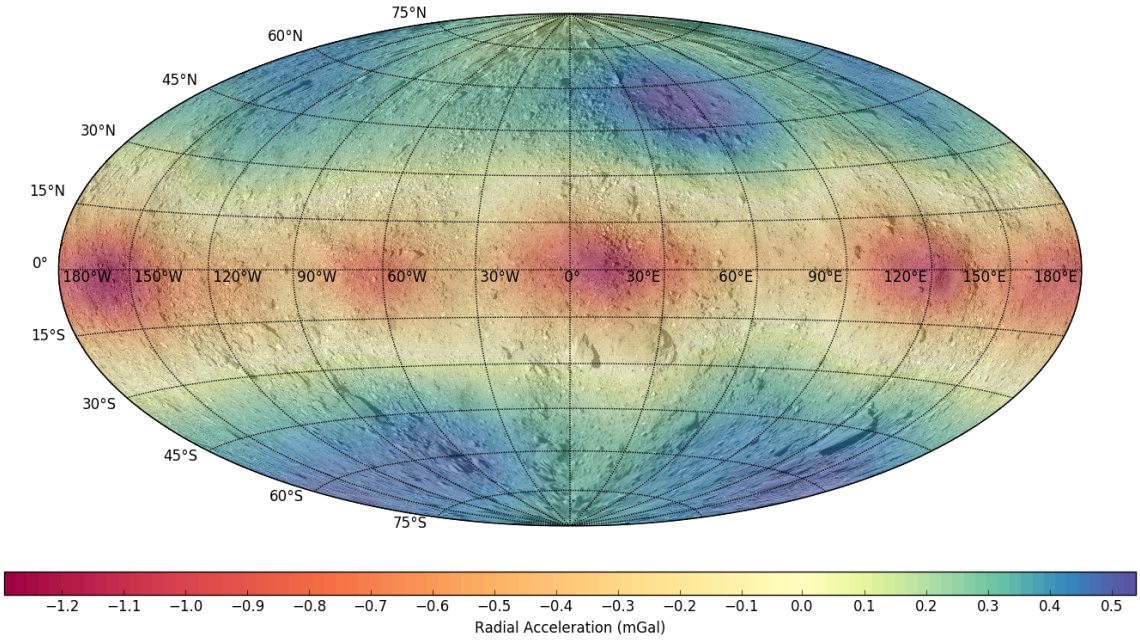

Figure 3: Radial gravity acceleration disturbance based on the constant density polyhedral shape model evaluated at 290 m from the center of Bennu.

A majority of the Orbital A phase would be conducted at distances from Bennu's center ranging from about 1.6 to 2.1 km. The sensitivity of the trajectory to the gravity field at these distances would allow for initial estimates of the degree 2 terms of the gravity field. Figure 4 shows the radial gravity acceleration at a 1.6 km sphere from the center of Bennu with the point-mass gravity removed. The gravity acceleration variation over the surface of the sphere ranges from -5.33×10^{-12} km/sec^2 to 8.00×10^{-12} km/sec^2. By estimating only a 2x2 gravity field during Orbital A, the expected residual error in the acceleration based on a truncated spherical harmonic model would produce a maximum acceleration error of about 4.0×10^{-13} km/sec^2 near the north pole. This acceleration error would be less than the amount detectable.

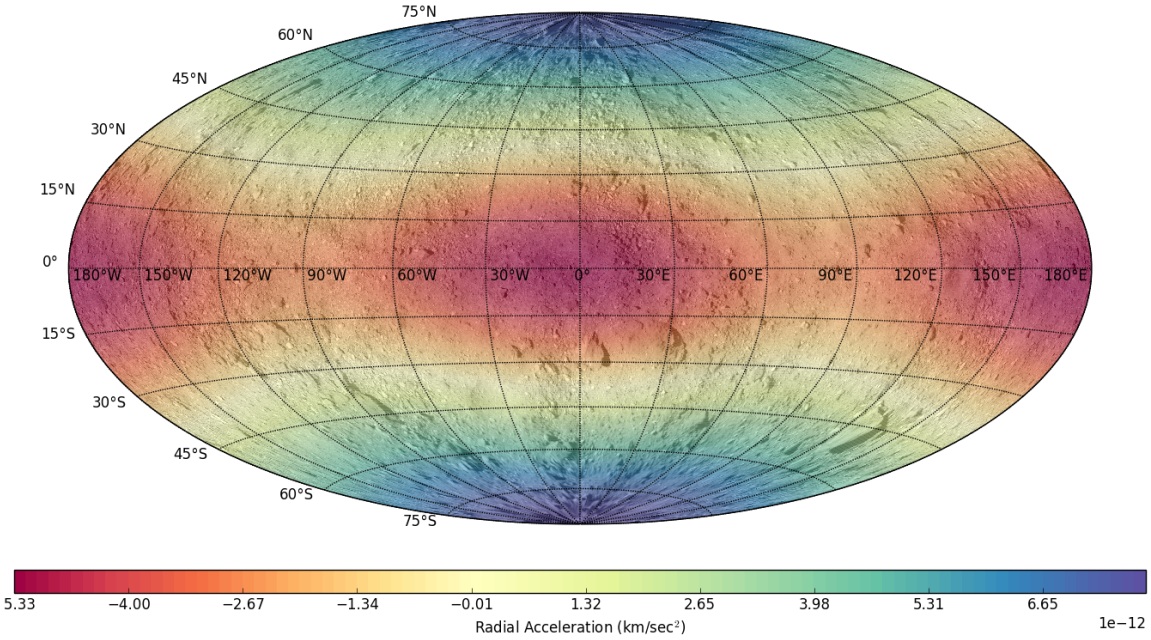

Figure 4: Radial gravity acceleration at a distance of 1.6 km from the center of Bennu, the Orbital A periapsis radius.

PRELIMINARY SURVEY

Bennu GM Estimation

The primary goal of the Preliminary Survey phase from the Navigation Team's perspective was to obtain an estimate of the mass of Bennu for updated orbit insertion designs for the following Orbital A phase. Pre-launch analysis showed that the uncertainty in the estimate of Bennu's GM could be obtained on the 1-2% level of the true value after the completion of the Preliminary Survey phase.[3] Prior to the start of ProxOps, the Preliminary Survey campaign was modified to include two additional north pole flybys to alleviate potential navigation errors in delivered trajectories for science observations and planning. These additional flybys helped to reduce the GM uncertainty and trajectory uncertainties prior the first prime science imaging on the third north pole flyby.

During the approach to Bennu, the OD team re-estimated the SRP specular and diffuse parameters for the defined 10-plate OSIRIS-REx spacecraft model. The goal of this updated modeling was to better predict the Sun-point and nadir-point attitudes that would be flown during the Preliminary Survey phase. During that later portion of Approach, the OpNav measurements enabled the spacecraft trajectory to be estimated on the order of 10's of meters of uncertainty rather than the 100's of m to km level of uncertainty seen throughout outbound cruise. This reduction of uncertainty due to the OpNavs allowed for more refined estimates of the SRP modeling. Trending of spacecraft trajectory prediction performance due to the updated modeling leading into the Preliminary Survey phase gave confidence that the SRP at the Sun-point attitude was well characterized. There was indication early on that, depending on how far off the Sun was from the $-$Z deck when the spacecraft was at nadir-point, the SRP modeling of the 10-plate calibrated model was not sufficient. However, the first four flybys would be at a combination of Sun-point and nadir-point where the Sun was almost directly on the $+$X face of the spacecraft (the common orientation seen in Sun-point, though the attitude could be rotated around this vector due to the nadir slewing and how far out of the terminator the spacecraft was during the flyby). The enhanced trajectory prediction performance late in Approach and alternate trajectory solution trending gave confidence to remove any stochastic acceleration modeling throughout the flybys.

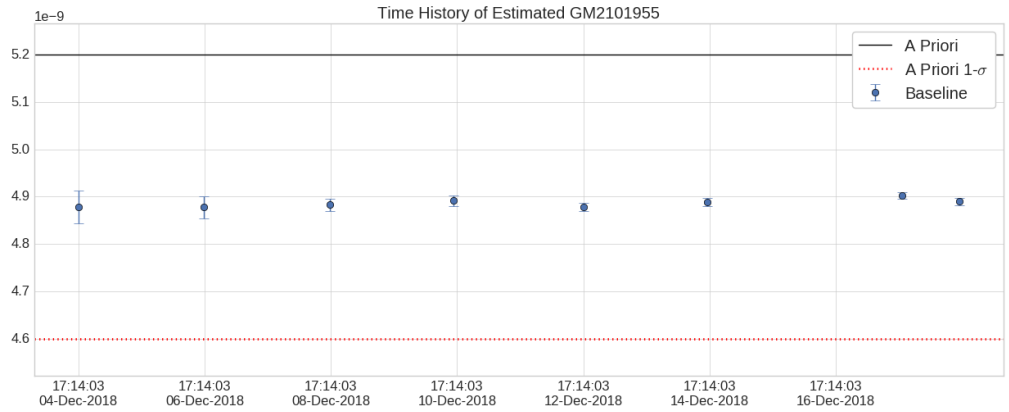

Figure 5: Evolution of Bennu GM estimates during the Preliminary Survey phase.

The first direct measurement of Bennu's mass occurred during the first half of the first north pole flyby. Using Doppler, range, and center-finding OpNav images based on updated shape models built on Approach, the GM of Bennu was estimated to be 4.879 ± 0.034 m^3/s^2. As each flyby was completed, additional data reduced the uncertainty in the estimate of the GM. Figure 5 shows the estimated solutions for Bennu's GM over the course of each Preliminary Survey flyby and OD solution. Estimates of Bennu's GM were obtained with data just prior to each close approach ($\sim$7.25 km from the center of Bennu). OD077, the final OD of Preliminary Survey after maneuver M7P, used tracking data throughout all of Approach and through every Preliminary Survey flyby in a single arc, and estimated the GM of Bennu to be 4.890 ± 0.007 m^3/s^2. This value for Bennu's GM was supplied to the Radio Science Working Group (RSWG) and used in the initial characterization of Bennu's geophysical environment.[38] Several variations in the estimation of Bennu's GM, such as data arc length, filtering techniques, and the use of a multi-arc filter, were used as validation of the final GM estimate prior to the design of the Orbital A insertion.[39]

Flyby Reconstruction and Prediction Performance

The OD schedule for the Preliminary Survey phase was such that roughly 24 hours after each burn that initiated a science leg, the OD team would produce a reconstructed trajectory just prior to the closest approach utilizing OpNav data up until 10:38 UTC with radio tracking data up to 17:00 UTC (the close approach time). This trajectory would then be used for the next maneuver design and would be put on-board the spacecraft just prior to the execution of the subsequent burn. The predicted trajectory would then last on-board through the subsequent flyby and up to the following maneuver three days later. This cycle would repeat itself throughout Preliminary Survey. The science observation planning for this phase utilized expected maneuver dispersions and OD performance based on pre-encounter covariance analysis.[3]

Trajectory prediction performance was tracked throughout Preliminary Survey by comparing the most recent OD trajectory prediction to the most recent OD trajectory reconstruction. Typical performance showed less than 1-sigma of the expected performance based on the ProxOps covariance analysis done prior to Approach. Upon completion of the Preliminary Survey phase, each trajectory prediction made during the phase was compared to the final reconstructed trajectory obtained through tracking data from the start of Approach through the beginning of Orbital A. Figure 6 shows that trajectory prediction performance in the Bennu-centered radial, transverse, and normal reference frame relative to the final reconstructed trajectory of Preliminary Survey. Figure 6 contains representative events after the data cut-off (DCO) that could occur in the predicted span of the trajectory. Science Flyby 1 is the first close approach after the DCO followed by Maneuver 1 which targeted Science Flyby 2. OD070 was the first trajectory delivery after Approach that contained the first half of the first north pole flyby, while OD075 was the last trajectory delivery prior to the final south pole flyby just prior to the execution of M7P. Each trajectory is predicted over 3.5 days since the last OpNav was shuttered at 10:38 UTC. This three day prediction contains the close approach flyby at 17:00 on that day, the subsequent maneuver to initiate the next leg, and the next science flyby up to the second

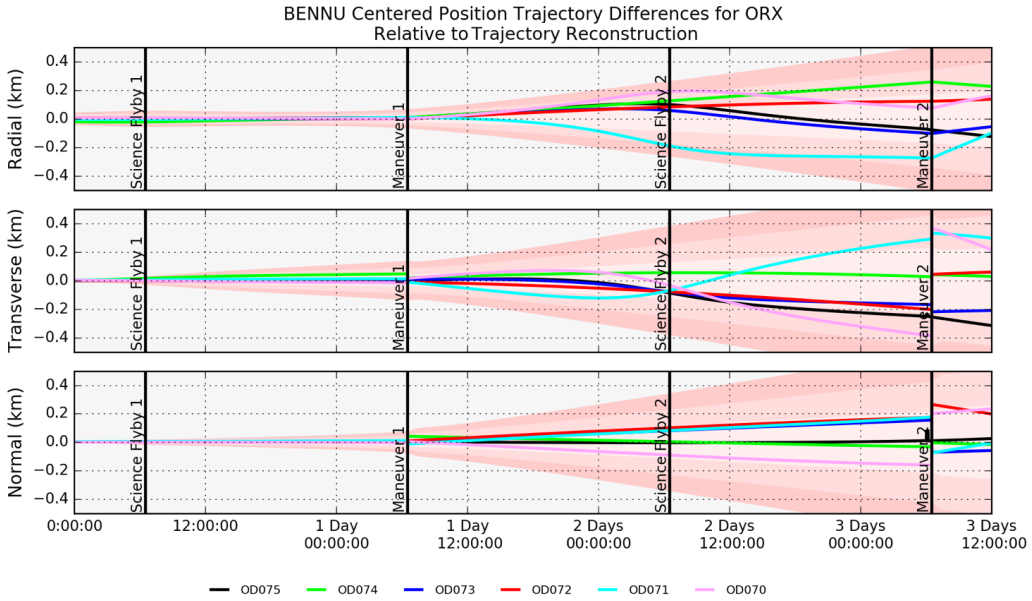

Figure 6: Preliminary Survey post DCO trajectory prediction vs reconstruct

maneuver in the sequence just prior to when the next ephemeris is uplinked to the spacecraft. OD072 and OD074 were transit leg predictions and did not have science flyby close approaches, though their prediction performance relative to the DCO provided insight for the subsequent OD.

Table 1 provides the in-flight predicted performance of the delivered OD trajectories throughout each of the maneuver and flyby events after their respective DCOs. The absolute errors in the radial, transverse, and normal are provided as minimum, mean, and maximum errors along with the 1.0, 50.0, and 99.0 percentile of the states. The main errors of concern are those of the OD error at the time of Maneuver 1 immediately following the DCO as well as the subsequent errors during science flyby 2 where the science imaging would take place. During the Maneuver 1 timeframe, the OD prediction was on average 4.683 m, 15.193 m, and 5.439 m in radial, transverse, and normal respectively. Through the science flyby 2 timeframe, the OD prediction was on average 124.474 m, 67.638 m, and 60.437 m in radial, transverse, and normal respectively. A majority of the prediction error for the science flyby originated from the maneuver performance. The only requirement for they flybys in this phase was to predict at the time of science flyby 2 to within ± 200 m 1-sigma in the radial direction.

Table 1: Preliminary Survey prediction performance after the last OpNav was shuttered.

	Post DCO Event	Min	Mean	Max	$\mathbf{P}_{1.0}$	$\mathbf{P}_{50.0}$	$\mathbf{P}_{99.0}$
Radial (m)	Science Flyby 1	1.714	7.357	21.887	1.795	4.997	21.154
	Maneuver 1	0.464	4.683	9.529	0.472	4.472	9.479
	Science Flyby 2*	58.069	124.474	190.884	59.321	112.608	190.818
	Maneuver 2	75.477	151.909	274.580	75.573	112.810	273.770
Transverse (m)	Science Flyby 1	0.135	4.585	14.916	0.180	2.962	14.445
	Maneuver 1	0.745	15.193	46.148	0.777	13.631	44.621
	Science Flyby 2*	34.284	67.638	87.359	35.316	74.562	86.999
	Maneuver 2	26.045	222.377	388.374	33.206	229.619	383.522
Normal (m)	Science Flyby 1	0.656	2.534	5.557	0.668	2.283	5.455
	Maneuver 1	0.868	5.439	11.501	1.003	4.290	11.331
	Science Flyby 2*	3.420	60.437	101.295	3.441	81.986	100.736
	Maneuver 2	10.295	118.171	176.600	11.390	157.549	176.511

* Not valid for OD072 and OD074 since they were transit legs and the close approach was not for science imaging.

ORBITAL A

Transition to the Orbital A phase occurred following the M1A burn that negated the final drift after the Preliminary Survey south pole flyby by putting the spacecraft on a trajectory that left the terminator and traversed the sunlit side of Bennu. This reverse drift was designed to enable a reduction in the spacecraft state uncertainties by utilizing the parallax in the OpNav images to shrink the large transverse uncertainties obtained from the drifting and maneuver performance. This allowed for a reduction in the predicted trajectory uncertainties through the orbital insertion sequence of M2B and M3B. The M3B insertion point was targeted to occur over the north pole of Bennu just behind the terminator plane so that OSIRIS-REx could enter into a stable maintenance-free frozen orbit.[40]

Once in orbit, the OD team began working on the transition from center-finding to landmark-based navigation. This transition utilized the extensive field-of-view (FOV) of the Touch and Go Camera System (TAGCAMS) NavCam 1 (Reference 15) to take a long exposure image of the stars followed by a short exposure image to resolve Bennu and its surface features. This technique allowed for the pointing of the camera to be obtained with the stellar image and applied to the resolved image of Bennu, alleviating the need to estimate a pointing correction to each image. An added benefit of this technique was that it allowed for the evaluation of the pointing solution accuracies of the on-board star trackers to ensure camera pointing used in future phases, where stellar images were not taken, would be sufficiently accurate. A set of criteria was established in order for the OD team to rigorously determine the accuracy of the landmarks and the ability to successfully transition from using center-finding OpNavs to landmark-based OpNavs as the baseline for all future ProxOps phases. The general navigation transition phase criteria are outlined as:

- Predicted trajectory state errors meet the accuracies required for Detailed Survey science observations
- Landmark-based predicted trajectories have improved over star-based predicted solutions
- Landmark-based reconstructed trajectories improved over star-based reconstructed solutions
- Landmark residuals have converged and are consistent with shape model requirements
- Bennu geophysical parameters have converged to within expected uncertainties

Insertion Reconstruction

The orbit insertion sequence for Orbital A began after the final south pole flyby of Preliminary Survey with the M1A maneuver to reverse the drift and reach the staging point of the M2A maneuver. The M2A maneuver would occur at a fixed time of 29 December 2018 at 17:00 UTC. This staging point allowed for the accurate targeting of the insertion burn, M3A, to occur above Bennu's north pole. Initial Monte-Carlo trajectory analysis showed that the M2A burn could put the spacecraft in a dispersed area above the north pole, requiring a variable maneuver time to accurately perform the insertion burn at the necessary point to achieve a frozen orbit. The nominal execution time of the M3A insertion maneuver was 31 December 2018 at 20:00 UTC. From a navigation perspective, the nominal design of the orbit insertion sequence was modified from that previously presented.[3,41] Initially, the spacecraft would drift after the final flyby in Preliminary Survey out to a staging point roughly 150 km from Bennu before reversing direction and staying in the terminator plane, targeting one of the poles of Bennu. This trajectory had large uncertainties even during reconstructed portions due to the geometry relative to Bennu and limited radial and transverse state knowledge. The insertion sequence was redesigned to fly the spacecraft in front of Bennu to a new staging point on the opposite side of Bennu to reduce the state uncertainties prior to orbit insertion (for more detail see Reference 40).

The hyperbolic nature of the trajectories leading up to the orbit insertion allowed for B-plane targets and parameters to be used as a reference of the trajectory performance relative to the desired targets. Figure 7 shows the expected maneuver performance of the M1A late update and its target as well as the subsequent OD deliveries that were made to reconstruct the trajectory mapped to a B-Plane at closest approach of the reverse drift trajectory in front of Bennu. OD078 and OD079 had DCOs 1 and 2 days after the M1A maneuver, resulting in the initial reconstructions of that maneuver with uncertainties of roughly 180 m in B·R and B·T with a time of closest approach uncertainty of 38 minutes. OD080's DCO was 1 week after the M1A burn and was 1 day prior to the closest approach of the hyperbolic transfer to the M2A point. At this time, a reduction in the B-plane position was obtained from the initial realization of parallax in the OpNav imaging

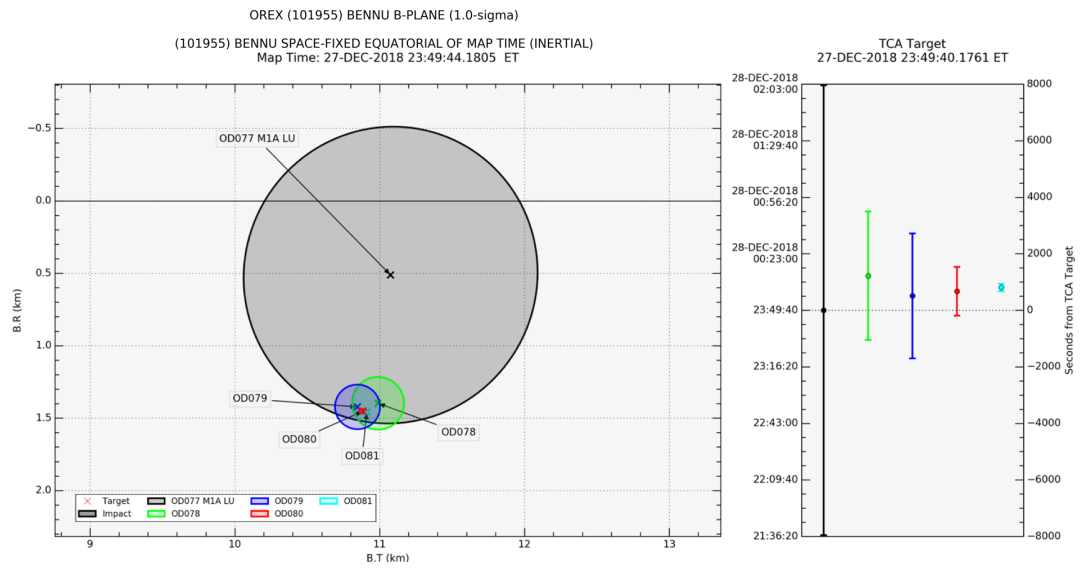

Figure 7: M1A B-plane target and subsequent reconstructions.

by traversing the sunlit side of Bennu. The B-plane position uncertainty was reduced to 30 m by this point with a time of close approach uncertainty of 14 minutes. OD081 was the late update OD used to design the final implementation of the M2A burn. The transit along the sunlit side of Bennu was completed by this point and we saw a significant reduction in the B-plane reconstruction uncertainty of 3 m with a time of closest approach uncertainty of 2 minutes. Figure 7 also shows that the predicted trajectory errors from OD to OD were stable and within 1-sigma shifts between deliveries, indicating that the predicted trajectories were well within the expected dispersion modeling.

Upon the completion of the M2A burn targeting the M3A insertion location, another OD late update was necessary. This late updated achieved two objectives: 1) it enabled the trajectory and maneuver teams to accurately redesign the frozen orbit parameters necessary to achieve a stable orbit; and 2) it allowed for an estimate of a time shift of when that burn should execute on-board the spacecraft. OD082 was delivered with data up to 24 hours after the execution of M2A. Initial radio-only data reconstructs of the M2A burn were done, but limited geometry and quantity of Doppler data provided limited insight into the burn execution. Figure 8 shows the delivered OD082 solution for the orbit insertion sequence as well as other filter cases that were evaluated against the nominal trajectory solution delivered to the Maneuver Team. OD082 modified the burn execution time of M3A from 20:00 UTC to 19:44 UTC on 31 December 2018.

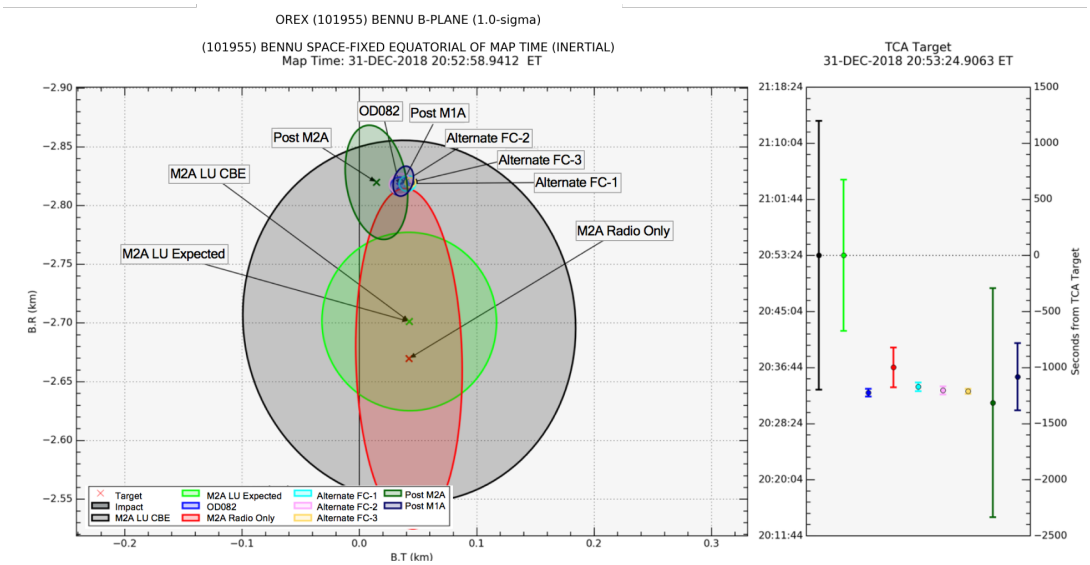

Figure 8: M2A B-plane target and subsequent reconstructions.

Landmark Transition

The Orbital A OpNav transition phase began on 31 December 2018 and lasted until 25 January 2019 with the first operational landmark-based trajectory solution delivered on 14 January 2019. Pre-launch analysis assumed that the center-finding optical data would be good to 1 pixel + 1% of the asteroid diameter. These values were based on past experience with optical center-finding techniques. For Orbital A, the average 1-sigma weighting applied for covariance analysis prior to ProxOps was around 10 pixels. The actual performance of the center-finding technique seen in Orbital A, as shown in Figure 9, was less than 0.5 pixels (or about 30 cm) 1-sigma. This equates to about 0.06% of the body diameter, reducing the pre-launch performance assumptions by 20 times. The performance and reliability of the center-finding OpNavs became so good that variations in the residuals due to shifted estimates in the pole solution could be seen in the image registration process (left vs. right side of Figure 9) as well as the center-of-figure to center-of-mass offset. The center-finding OpNavs exceeded all performance expectations providing a good baseline for comparing solutions to landmark-based estimates.

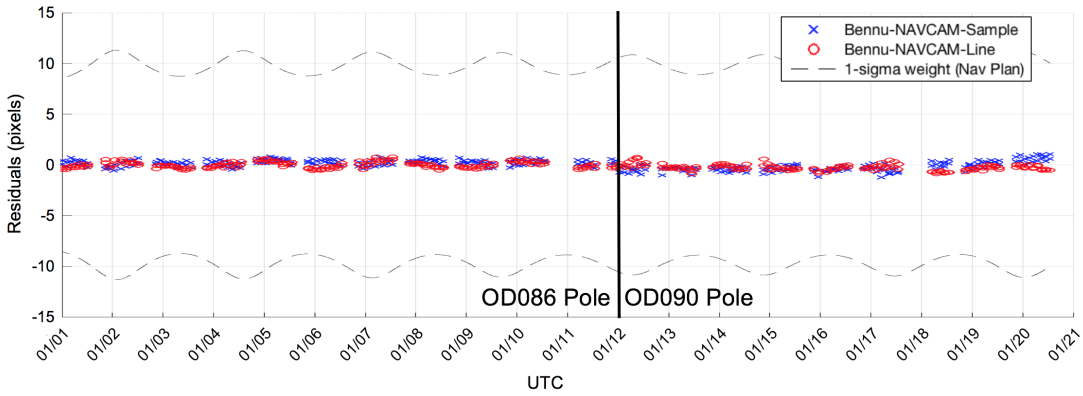

Figure 9: Center-finding OpNav performance throughout Orbital A.

The exceptional performance of the center-finding OpNavs was due in part to updated techniques in processing optical images developed by the OpNav team in their KXIMP software as well as early shape model deliveries from the ALTWG. This increased performance made the criteria for transitioning to landmark-based navigation (mainly the reconstructed vs predicted accuracies) more difficult to assess. One indication of improved performance in the landmark solutions was better consistency between OD solutions in the reconstructed trajectory that fell within the *a posteriori* covariance, while reconstructed trajectory solutions from center-finding OpNavs could typically lie well outside 3-sigma of the *a posteriori* covariance of the landmark-based solution, though the solutions were statistically consistent based on their combined uncertainties. The defining factor of the landmark transition success was based on the predicted performance of the solutions. Center-finding OD solutions typically had errors at the 10 m, 20 m and 5 m level in radial, transverse and normal respectively over 24 hours, while the landmark-based solutions' prediction errors were 5 m, 10 m, and 2 m. This marked the end of the landmark transition phase.

Bennu Shape and Landmark Estimates

As part of the transition to landmark navigation, the OD team began estimating the landmark locations, a frame rotation offset between the shape model frame and the spin axis, a center-of-figure to center-of-mass offset, landmark scaling, rotation rate, and the associated right ascension, declination, and prime meridian relative to the ICRF. In nominal operations during Orbital A, the shape model provided by the ALTWG had 1.5 m and 75 cm resolution landmarks globally with a subset of 35 cm resolution landmarks. The shape model and landmark locations were used as provided except for estimating a parameter to scale all of the landmarks and a center-of-figure to center-of-mass offset. The wide FOV of NavCam 1 allowed large portions of Bennu's surface to be correlated to landmarks in each image. However, systematic biases in landmark locations were suspected to be influencing the estimated pole parameters.

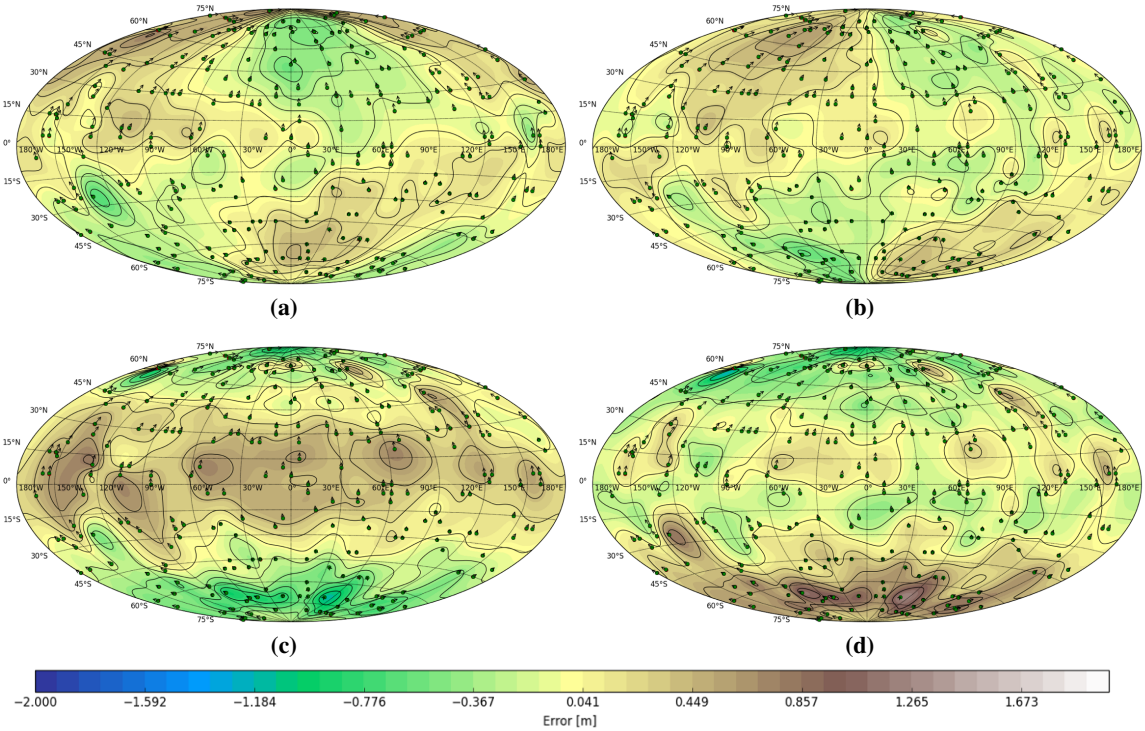

Figure 10: Estimated shifts in the ALTWG shape model landmark locations for (a) the body-fixed X direction, (b) the body-fixed Y direction, (c) the body-fixed Z direction, and (d) the altitude.

The OD team estimated a set of about 200 landmarks covering the surface utilizing a subset of landmarks that were seen in a majority of the images. The locations of these landmarks were estimated simultaneously with the nominal trajectory estimation. Figure 10 shows the results of the landmark vector shifts in the Bennu body-fixed frame X (Figure 10a), Y (Figure 10b), and Z (Figure 10c) directions, as well as the local altitude (Figure 10d) correction of that landmark, with the mean shift of all the landmarks removed relative to their original locations reported by the ALTWG. Regional variations can be seen in the X and Y coordinates. Of particular note is the Z correction near the poles. Figure 10c indicates that the landmark locations needed to be shifted -70 cm. The overall model saw corrections in landmark locations of less than 1.5 m across the globe. An important consequence of estimating the landmark locations was a shift in the location of the prime meridian or spin axis (body-fixed Z direction). The OD team alleviated this issue by anchoring one landmark location or estimating a frame offset rotation between the shape-model-defined frame and the spin axis.

Figure 11 shows the distribution of shifts in the landmark vectors in the X, Y, and Z directions. The average shifts in each direction are considered to be a correction from the center-of-mass to the current location of the shape model origin (center-of-figure). The average landmark offset correction for this ALTWG shape model was determined to be -5 cm in X, 8 mm in Y, and 49 cm in Z. The minute correction in X and Y is due to the fact that the offset was observed early on in the mission due to the modulation in the landmark locations in the images, while the Z component could only be observed to sufficient accuracy once in a closed orbit. This shape model offset correction, however, is not the offset from the center-of-volume (the center of the model assuming a constant density), but rather the current correction between the observed center-of-mass of Bennu inferred from the trajectory dynamics and the location of the defined center-of-figure of the shape model.

Every OD delivery made in Orbital A used the ALTWG model as is without correcting the landmark locations. The typical shape model residuals throughout Orbital A were about 0.4 pixels 1-sigma (a resolution of about 16 cm to 22 cm on the surface) in both the sample and line direction of the NavCam 1 imager (Figure 12a). When correcting the landmark locations based on the estimation of the landmarks previously described, the landmark residuals were reduced to 0.2 pixels 1-sigma (a resolution of about 8 cm to 11 cm on the surface) in the sample and line direction of the NavCam 1 imager (Figure 12b).

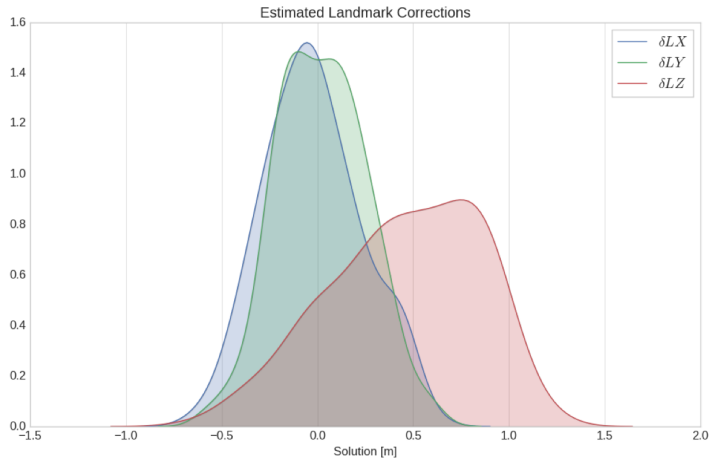

Figure 11: Histogram kernel density function of the estimated landmark shifts in the body-fixed X, Y, and Z directions.

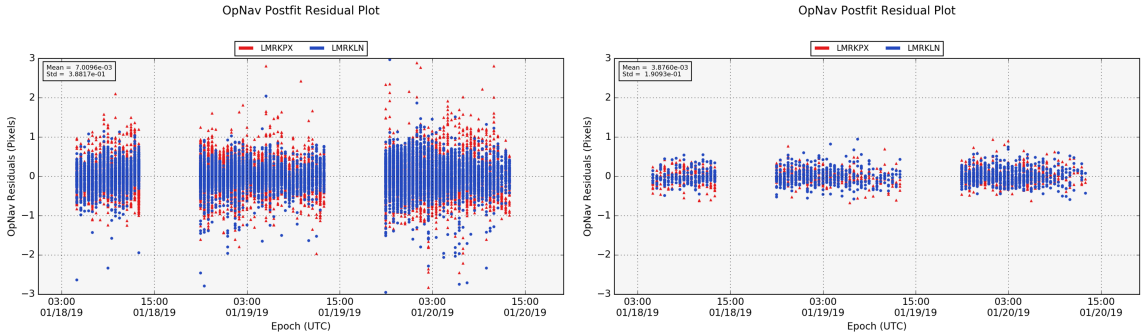

(a) **(b)**

Figure 12: ALTWG 35-cm shape model residuals obtained in Orbital A. (a) is the shape model landmark residuals as is. (b) is the landmark residuals with corrected landmark locations.

Bennu GM refinement and gravity estimation

Orbital A provided the closest distance to Bennu during the Navigation Campaign, allowing for refinement of parameter estimates such as the mass of Bennu. Figure 13 shows the evolution of the GM estimates obtained from the baseline filter strategy that was delivered throughout Orbital A. The Bennu GM *a priori* value and uncertainty of 5.2 ± 0.6 m^3/s^2 is not visible in Figure 13 due to the spread of the estimated GM and *a posteriori* uncertinaty. Immediately following orbit insertion, a spike in the estimate of the GM was

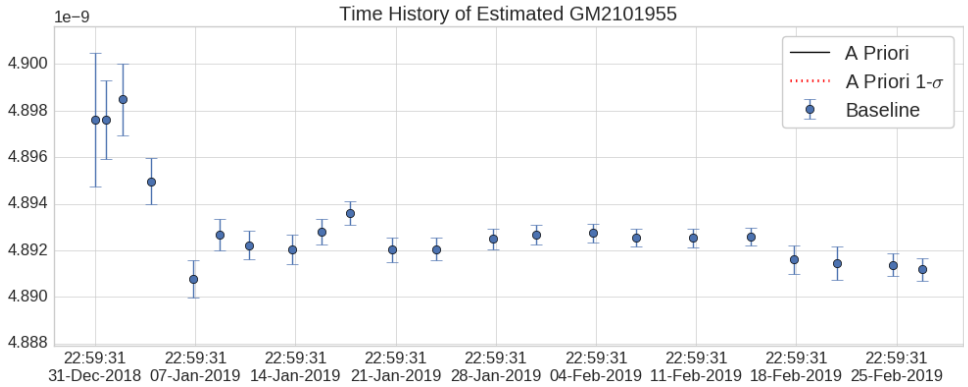

Figure 13: History of GM estimates throughout the Orbital A deliveries with 1-sigma error bars.

noticed; however, the belief was that this was aliased with the maneuver estimates and initial structure of the tracking data post-insertion. Once an orbital revolution (62 hours) was completed, the estimates for the GM remained rather consistent for the remainder of Orbital A. Estimated values typically varied within 1-sigma of their estimated uncertainties from solution to solution and were statistically consistent with those obtained in Preliminary Survey.

Degree 2 spherical harmonics were not observable throughout Orbital A with the *a posteriori* uncertainty in the estimated parameters having a signal-to-noise ratio (SNR) < 3. The second degree zonal harmonic, J_2, had a SNR of 25 by the end of Orbital A, with estimated values varying from solution to solution within the *a posteriori* uncertainty. This gave an indication that there was some mismodeling or aliasing in the dynamical model leading to a significant number of enhancements that were trended during the Orbital A phase in order to provide more accurate and consistent estimates of the gravity parameters.[12] The initial attempt of estimating a 2x2 gravity field during the Navigation Campaign provided insight into the weak gravitational dynamic environment of Bennu.

Pole Parameters and Evolution

Multiple rotation movies were taken of Bennu during the Approach phase to determine the inertial orientation of Bennu and its rotation rate. The narrow FOV imager PolyCam was used to create the rotation movies when the spacecraft was 162 km away from the asteroid with a resolution of 2.2 m/pix on the surface.[6] The images were taken about 7 minutes apart while the spacecraft was maintained in nadir-point (slewing on reaction wheels to maintain Bennu at the center of the FOV). From these movies, the rotation axis (right ascension and declination) and spin rate were determined to be 85.19 ± 0.26 deg, -60.3 ± 0.06 deg, and 2011.166 ± 0.012 deg/day.

A potential issue with the Approach imaging data set is that the spacecraft was not at inertial hold during the imaging; it was slewing to maintain nadir-point. To address this, the OD team had to estimate either per-image pointing corrections or a correlated time-history of pointing corrections. These pointing corrections directly impacted the accuracy of the pole estimate. During Orbital A, however, each landmark image taken was held in inertial hold and each image had a companion stellar OpNav, giving the orientation of the camera in inertial space decoupled from the noisy star-tracker-derived attitude estimation. This technique performed exceptionally well and allowed the OpNav team to trend the solutions obtained from the stellar pointing solution to the on-board star tracker solutions. Removing this potential image bias allowed for more consistent estimates of Bennu's pole. A frame offset was estimated to define the orientation of the instantaneous spin axis in the shape model frame. In general, no significant frame offset was detected and the principal $+$Z axis was well defined in the shape model frame by the time of Orbital A. Early in Approach, it was noticed that there could have been a significant offset of 0.2 degrees between the spin axis and the $+$Z axis defined by the shape model. However, through iteration with the ALTWG and updated pole estimates, the shape model frame $+$Z axis converged on the true spin axis.

Figure 14 provides the evolution of the right ascension and declination of Bennu's pole over the course of Orbital A. The final estimate of Bennu's pole based on OD103 using the landmarks in the ALTWG shape model as provided resulted in a right ascension and declination estimate of 85.58 ± 0.02 deg, -60.315 ± 0.007 deg. Due to the excessive number of landmarks, the uncertainties obtained from the OD103 solution

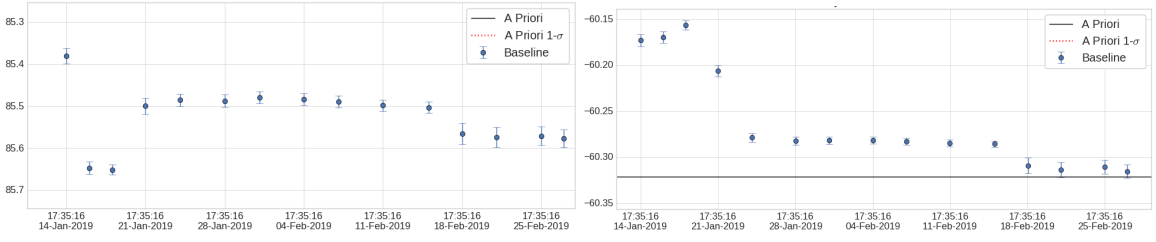

(a) **(b)**

Figure 14: Right ascension (a) and declination (b) variation as they were estimated throughout Orbital A with their respective DCOs with 1-sigma error bars.

seemed optimistic. The OD team knew that the landmarks in the ALTWG shape model were in error and that there were regional variations in the landmark errors that could influence the estimate of the pole. This was confirmed with the estimation of various subsets of landmarks for several shape model deliveries provided by ALTWG. When estimating the landmark locations, the pole for all solutions converged to 85.457 ± 0.007 deg, -60.365 ± 0.003 deg.

Prediction Performance

Trajectory ephemeris estimates were generated every Monday, Wednesday, and Friday throughout all of Orbital A with their trajectories getting on-board the spacecraft in a late update sequence just 24 hours after the DCO. Desaturation maneuvers (desats) to remove momentum from the reaction wheels were performed every Tuesday and Thursday. This operations cadence ensured that the Monday and Wednesday OD deliveries would only predict for 2 days limiting the desat errors to 24 hours of propagation. The Friday OD would fully reconstruct the previous Thursday desat to reduce prediction errors until the subsequent Monday OD delivery.

ProxOps covariance analysis prior to orbital insertion showed that the expected dispersions due to mismodeling could grow rapidly depending on desat magnitudes as well as uncertainties in the force modeling. These predicted errors could grow to be as much as 24 degrees 3-sigma in the transverse direction (about 880 m at 2.1 km radius) over 2 or 3 days depending on how close to the DCO the desat occurred. To ensure that a single image contained all of Bennu in the NavCam 1 FOV, a 2x1 mosaic was designed for use at the onset of Orbital A. Over the course of 2 days worth of prediction, the transverse error from the delivered OD solutions estimated in Orbital A onward were never greater than 110 m (3 degrees at 2.1 km) and on average were 15 m (0.5 degrees at 2.1 km). Figure 15 shows the predicted performance of every OD delivery made during the Orbital A phase. OD101 is an outlier when compared to the 7-day prediction spans of the other 25 OD deliveries made. In general, predicted ephemeris errors throughout all of the Orbital A campaign were less than 1-sigma of the anticipated predicted trajectory errors prior to ProxOps.

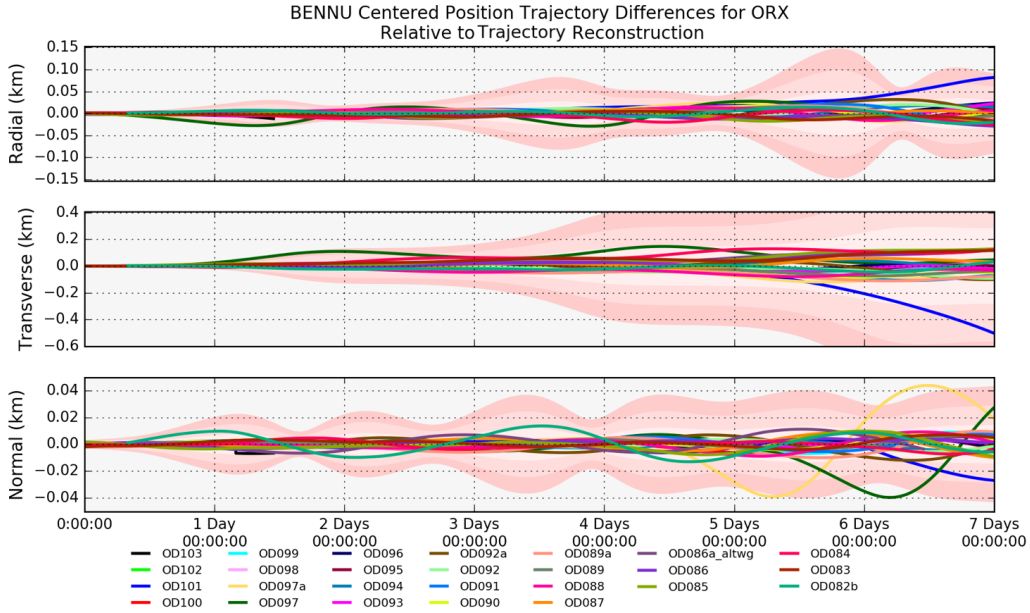

Figure 15: Orbital A prediction performance after the last OpNav was shuttered.

The predicted trajectory errors from delivered OD trajectories throughout Orbital A are provided in Table 2 relative to the last OpNav taken around 13:20 UTC every day. The absolute errors in the radial, transverse, and normal are provided as minimum, mean, and maximum errors along with the 1.0, 50.0, and 99.0 percentile of the states. Of main concern for the OD team were predictions over 1-, 2-, and 7-day timeframes. The 1- and 2-day prediction error provided insight into how well the OD predictions held up through the first HGA contact the day after the DCO, as did the general prediction errors over 48 hours until the next trajectory would go

on-board the spacecraft for nadir-relative pointing. In addition, the 1-day predictions did not include any desat in the predicted span while the 2-day predictions did. The desat during the Orbital A campaign were estimated to be 0.045 mm/sec 1-sigma in magnitude. The 7-day prediction errors are provided to give an indication as to how well the trajectory solutions would hold up over the course of multiple desat, predicted attitude errors, and force modeling errors in the long-term. For a 1-day prediction, the OD trajectory error was on average 2.532 m, 4.033 m and 1.384 m in radial, transverse, and normal respectively. The 2-day trajectory prediction errors on average were 3.232 m, 15.123 m, and 1.727 m. The 7-day prediction errors accumulated to 15.757 m, 78.267 m, and 7.095 m.

Table 2: Orbital A prediction performance after the last OpNav was shuttered.

	Duration	Min	Mean	Max	$\mathbf{P}_{1.0}$	$\mathbf{P}_{50.0}$	$\mathbf{P}_{99.0}$
Radial (m)	1 Day	0.041	2.532	22.537	0.043	1.581	18.359
	2 Days	0.177	3.232	11.464	0.268	2.088	10.653
	7 Days	0.856	15.757	82.007	0.943	13.499	70.336
Transverse (m)	1 Day	0.043	4.033	25.021	0.059	2.511	22.510
	2 Days	0.639	15.123	108.932	0.815	9.111	89.548
	7 Days	1.398	78.267	503.040	4.456	45.665	420.626
Normal (m)	1 Day	0.045	1.384	9.708	0.049	0.751	8.148
	2 Days	0.203	1.727	9.666	0.220	0.971	8.446
	7 Days	0.138	7.095	27.518	0.230	4.946	27.434

CONCLUSION

The OSIRIS-REx Navigation Team successfully completed the Navigation Campaign and transitioned to landmark-based navigation within the first two weeks after orbit insertion in the Orbital A phase. The trajectory prediction performance for every phase was typically less than 1-sigma of the pre-encounter covariance analysis. Initial spin-state estimation of the pole of Bennu was obtained through rotation movies in the Approach phase. The estimation of the spin-state was refined during Orbital A through increased resolution images as well as updated shape model maplets of the surface features. Early estimation of the GM of Bennu utilizing pre-encounter SRP trending enabled the OD team to accurately estimate the mass of Bennu during the first half of the first 7.25 km flyby of Preliminary Survey. This enabled improved prediction performance throughout Preliminary Survey and the design of the Orbital A insertion maneuver. Center-finding OpNav performance exceeded all pre-encounter expectations and made the transition to landmark-based navigation easier than anticipated. Estimation of landmark locations improved the precision of OD solutions and provided consistent estimates of Bennu's geophysical and spin-state parameters.

ACKNOWLEDGMENTS

The authors wish to acknowledge other members of the OSIRIS-REx team who have contributed to accomplishments described in this paper: the Lockheed Martin flight operations team with special emphasis on thermal analysis data provided by Chris May and support from Javier Cerna and the telecom team; the Altimetry Working Group for early shape model deliveries used in OpNav processing; and members of the Science Planning and Science Operations teams at the University of Arizona who have supported OpNav observation planning.

This material is based upon work supported by NASA under Contracts NNM10AA11C, NNG12FD66C, and NNG13FC02C. OSIRIS-REx is the third mission in NASA's New Frontiers Program. Dante Lauretta of the University of Arizona, Tucson, is the mission's Principal Investigator, and the University of Arizona also leads the Science Team and the science observation planning and data processing. Lockheed Martin Space Systems in Denver built the spacecraft and is providing flight operations. Goddard Space Flight Center and KinetX Aerospace are responsible for navigating the OSIRIS-REx spacecraft.

REFERENCES

[1] D. Lauretta, S. Balram-Knutson, E. Beshore, W. V. Boynton, C. D. d'Aubigny, D. DellaGiustina, H. Enos, D. Golish, C. Hergenrother, E. Howell, *et al.*, "OSIRIS-REx: sample return from asteroid (101955) Bennu," *Space Science Reviews*, Vol. 212, No. 1-2, 2017, pp. 925–984.

[2] D. Lauretta, A. Bartels, M. Barucci, E. Bierhaus, R. Binzel, W. Bottke, H. Campins, S. Chesley, B. Clark, B. Clark, *et al.*, "The OSIRIS-REx target asteroid (101955) Bennu: Constraints on its physical, geological, and dynamical nature from astronomical observations," *Meteoritics & Planetary Science*, Vol. 50, No. 4, 2015, pp. 834–849.

[3] B. Williams, P. Antreasian, E. Carranza, C. Jackman, J. Leonard, D. Nelson, B. Page, D. Stanbridge, D. Wibben, K. Williams, *et al.*, "OSIRIS-REx flight dynamics and navigation design," *Space Science Reviews*, Vol. 214, No. 4, article id 69, 2018.

[4] P. G. Antreasian, M. C. Moreau, C. D. Adam, A. French, J. Geeraert, K. M. Getzandanner, D. E. Highsmith, J. M. Leonard, E. J. Lessac-Chenen, A. H. Levine, *et al.*, "OSIRIS-REX Navigation Performance During the First Leg of Outbound Cruise," *AAS GNC Conference*, Breckenridge, CO, 2018.

[5] P. G. Antreasian, M. C. Moreau, C. D. Adam, A. French, J. Geeraert, K. M. Getzandanner, D. E. Highsmith, J. M. Leonard, E. J. Lessac-Chenen, A. H. Levine, *et al.*, "Early Navigation Performance of the OSIRIS-REx Approach to Bennu," *AAS Annual Guidance and Control Conference*, 2019.

[6] B. Rizk, C. D. d'Aubigny, D. Golish, C. Fellows, C. Merrill, P. Smith, M. Walker, J. Hendershot, J. Hancock, S. Bailey, *et al.*, "OCAMS: the OSIRIS-REx camera suite," *Space Science Reviews*, Vol. 214, No. 1, article id 26, 2018.

[7] C. D. Jackman, D. S. Nelson, L. K. Mccarthy, T. J. Finley, A. J. Liounis, K. M. Getzandanner, P. G. Antreasian, and M. C. Moreau, "Optical Navigation Concept of Operations for the Osiris-Rex Mission," *AAS/AIAA Spaceflight Mechanics Meeting*, 2017.

[8] E. Mazarico, D. D. Rowlands, T. J. Sabaka, K. M. Getzandanner, D. P. Rubincam, J. B. Nicholas, and M. C. Moreau, "Recovery of Bennu's orientation for the OSIRIS-REx mission: implications for the spin state accuracy and geolocation errors," *Journal of Geodesy*, Vol. 91, No. 10, 2017, pp. 1141–1161.

[9] P. Antreasian, M. Moreau, C. Jackman, K. Williams, B. Page, and J. Leonard, "OSIRIS-REx Orbit Determination Covariance Studies at Bennu," *39th Annual AAS Guidance and Control Conference*, Breckenridge, CO, February 05, 2016 - February 10, 2016; AAS 16-101 2016.

[10] S. R. Chesley, D. Farnocchia, M. C. Nolan, D. Vokrouhlickỳ, P. W. Chodas, A. Milani, F. Spoto, B. Rozitis, L. A. Benner, W. F. Bottke, *et al.*, "Orbit and bulk density of the OSIRIS-REx target Asteroid (101955) Bennu," *Icarus*, Vol. 235, 2014, pp. 5–22.

[11] J. M. Leonard, P. G. Antreasian, C. D. Jackman, B. Page, D. R. Wibben, and M. C. Moreau, "Orbit Determination Strategy and Simulation Performance for OSIRIS-REx Proximity Operations," *10th International ESA Conference on Guidance, Navigation and Control Systems*, May 29, 2017 - June 02, 2017; Salzburg; Austria, 2017.

[12] J. Geeraert, J. Leonard, P. Kenneally, C. May, P. Antreasian, M. Moreau, and D. Lauretta, "OSIRIS-REx Navigation Small Force Models," *AAS/AIAA Astrodynamics Specialist Conference, Portland, Maine*, 2019.

[13] O. Barnouin, M. Daly, E. Palmer, R. Gaskell, J. Weirich, C. Johnson, M. Al Asad, J. Roberts, M. Perry, H. Susorney, *et al.*, "Shape of (101955) Bennu indicative of a rubble pile with internal stiffness," *Nature geoscience*, Vol. 12, No. 4, 2019, p. 247.

[14] J. Y. Pelgrift, E. M. Sahr, D. S. Nelson, C. D. Jackman, L. Benhacine, B. J. Bos, B. Rizk, C. d'Aubigny, D. Golish, D. DellaGiustina, *et al.*, "In-flight calibration of the OSIRIS-REx optical navigation imagers," *1st Annual RPI Workshop on Image-Based Modeling and Navigation for Space Applications. RPI*, 2018.

[15] B. Bos, M. Ravine, M. Caplinger, J. Schaffner, J. Ladewig, R. Olds, C. Norman, D. Huish, M. Hughes, S. Anderson, *et al.*, "Touch and Go Camera System (TAGCAMS) for the OSIRIS-REx asteroid sample return mission," *Space Science Reviews*, Vol. 214, No. 1, article id 37, 2018.

[16] C. Jackman and P. Dumont, "Optical navigation capabilities for deep space missions," *Proceedings of the 23rd AAS/AIAA Space Flight Mechanics Conference*, 2013.

[17] D. S. Nelson, E. J. Lessac-Chenen, J. Y. Pelgrift, C. D. Adam, F. J. Pelletier, *et al.*, "Optical Navigation Preparations for the New Horizons Kuiper-Belt Extended Mission," *1st Annual RPI Workshop on Image-Based Modeling and Navigation for Space Applications. RPI*, 2018.

[18] R. Gaskell, O. Barnouin-Jha, D. J. Scheeres, A. Konopliv, T. Mukai, S. Abe, J. Saito, M. Ishiguro, T. Kubota, T. Hashimoto, *et al.*, "Characterizing and navigating small bodies with imaging data," *Meteoritics & Planetary Science*, Vol. 43, No. 6, 2008, pp. 1049–1061.

[19] M. Ziebart, S. Edwards, S. Adhya, A. Sibthorpe, P. Arrowsmith, and P. Cross, "High precision GPS IIR orbit prediction using analytical non-conservative force models," *ION GNSS*, 2004, pp. 1764–1770.

[20] P. Steigenberger, S. Thoelert, and O. Montenbruck, "GNSS satellite transmit power and its impact on orbit determination," *Journal of Geodesy*, Vol. 92, Jun 2018, pp. 609–624, 10.1007/s00190-017-1082-2.
[21] A. Heilmann, L. D. D. Ferreira, C. Dartora, and K. Nobrega, "Perturbative effects of antenna radiation reaction on artificial satellite orbit," *Aerospace Science and Technology*, Vol. 23, No. 1, 2012, pp. 352–357.
[22] L. A. Lebofsky, M. V. Sykes, E. F. Tedesco, G. J. Veeder, D. L. Matson, R. H. Brown, J. C. Gradie, M. A. Feierberg, and R. J. Rudy, "A refined "standard" thermal model for asteroids based on observations of 1 Ceres and 2 Pallas," *Icarus*, Vol. 68, No. 2, 1986, pp. 239–251.
[23] A. W. Harris, "A thermal model for near-Earth asteroids," *Icarus*, Vol. 131, No. 2, 1998, pp. 291–301.
[24] D. DellaGiustina, J. Emery, D. Golish, B. Rozitis, C. Bennett, K. Burke, R.-L. Ballouz, K. Becker, P. Christensen, C. D. d'Aubigny, *et al.*, "Properties of rubble-pile asteroid (101955) Bennu from OSIRIS-REx imaging and thermal analysis," *Nature Astronomy*, Vol. 3, No. 4, 2019, p. 341.
[25] J. R. Spencer, L. A. Lebofsky, and M. V. Sykes, "Systematic biases in radiometric diameter determinations," *Icarus*, Vol. 78, No. 2, 1989, pp. 337–354.
[26] M. C. Nolan, C. Magri, E. S. Howell, L. A. Benner, J. D. Giorgini, C. W. Hergenrother, R. S. Hudson, D. S. Lauretta, *et al.*, "Shape model and surface properties of the OSIRIS-REx target Asteroid (101955) Bennu from radar and lightcurve observations," *Icarus*, Vol. 226, No. 1, 2013, pp. 629–640.
[27] B. E. Clark, R. P. Binzel, E. S. Howell, E. A. Cloutis, M. Ockert-Bell, P. Christensen, M. A. Barucci, F. DeMeo, D. S. Lauretta, H. Connolly Jr, *et al.*, "Asteroid (101955) 1999 RQ36: Spectroscopy from 0.4 to 2.4 μm and meteorite analogs," *Icarus*, Vol. 216, No. 2, 2011, pp. 462–475.
[28] D. Lauretta, D. DellaGiustina, C. Bennett, D. Golish, K. Becker, S. Balram-Knutson, O. Barnouin, T. Becker, W. Bottke, W. Boynton, *et al.*, "The unexpected surface of asteroid (101955) Bennu," *Nature*, Vol. 568, No. 7750, 2019, p. 55.
[29] C. W. Hergenrother, M. C. Nolan, R. P. Binzel, E. A. Cloutis, M. A. Barucci, P. Michel, D. J. Scheeres, C. D. d'Aubigny, D. Lazzaro, N. Pinilla-Alonso, *et al.*, "Lightcurve, color and phase function photometry of the OSIRIS-REx target asteroid (101955) Bennu," *Icarus*, Vol. 226, No. 1, 2013, pp. 663–670.
[30] N. H. Samarasinha and B. E. Mueller, "Component periods of non-principal-axis rotation and their manifestations in the lightcurves of asteroids and bare cometary nuclei," *Icarus*, Vol. 248, 2015, pp. 347–356.
[31] R. S. Hudson and S. J. Ostro, "Shape and non-principal axis spin state of asteroid 4179 Toutatis," *Science*, Vol. 270, No. 5233, 1995, pp. 84–86.
[32] D. P. Rubincam, "Radiative spin-up and spin-down of small asteroids," *Icarus*, Vol. 148, No. 1, 2000, pp. 2–11.
[33] M. C. Nolan, E. S. Howell, D. J. Scheeres, J. W. McMahon, O. Golubov, C. W. Hergenrother, J. P. Emery, K. S. Noll, S. R. Chesley, and D. S. Lauretta, "Detection of rotational acceleration of Bennu using HST light curve observations," *Geophysical Research Letters*, Vol. 46, No. 4, 2019, pp. 1956–1962.
[34] C. Hergenrother, C. Maleszewski, M. Nolan, J.-Y. Li, C. D. d'Aubigny, F. Shelly, E. Howell, T. Kareta, M. Izawa, *et al.*, "The operational environment and rotational acceleration of asteroid (101955) Bennu from OSIRIS-REx observations," *Nature communications*, Vol. 10, No. 1, 2019, p. 1291.
[35] D. Vokrouhlicky, W. F. Bottke, S. R. Chesley, D. J. Scheeres, and T. S. Statler, "The Yarkovsky and YORP effects," *Asteroids IV*, 2015, pp. 509–531.
[36] B. A. Archinal, M. F. A'Hearn, E. Bowell, A. Conrad, G. J. Consolmagno, R. Courtin, T. Fukushima, *et al.*, "Report of the IAU Working Group on Cartographic Coordinates and Rotational Elements: 2009," *Celestial Mechanics and Dynamical Astronomy*, Vol. 109, Feb 2011, pp. 101–135.
[37] D. J. Scheeres, S. Hesar, S. Tardivel, M. Hirabayashi, D. Farnocchia, J. W. McMahon, S. Chesley, O. Barnouin, R. Binzel, W. Bottke, *et al.*, "The geophysical environment of Bennu," *Icarus*, Vol. 276, 2016, pp. 116–140.
[38] D. Scheeres, J. McMahon, A. French, D. Brack, S. Chesley, D. Farnocchia, Y. Takahashi, J. Leonard, J. Geeraert, B. Page, *et al.*, "The dynamic geophysical environment of (101955) Bennu based on OSIRIS-REx measurements," *Nature Astronomy*, Vol. 3, No. 4, 2019, p. 352.
[39] A. French, J. Leonard, J. Geeraert, B. Page, P. Antreasian, M. Moreau, J. McMahon, D. Scheeres, and D. Lauretta, "Multi-Arc Filtering During the Navigation Campaign of The OSIRIS-REx Mission," *AAS/AIAA Astrodynamics Specialist Conference, Portland, Maine*, 2019.
[40] D. Wibben, A. Levin, S. Rieger, J. McAdams, P. Antreasian, J. Leonard, M. Moreau, and D. Lauretta, "OSIRIS-REx Navigation Campaign Trajectory Design and Maneuver Performance," *AAS/AIAA Astrodynamics Specialist Conference, Portland, Maine*, 2019.
[41] D. R. Wibben, K. E. Williams, J. V. McAdams, P. G. Antreasian, J. M. Leonard, and M. C. Moreau, "Maneuver Strategy for OSIRIS-REx Proximity Operations," *10th International ESA Conference on Guidance, Navigation and Control Systems*, May 29, 2017 - June 02, 2017; Salzburg; Austria, 2017.